



Trans. Nonferrous Met. Soc. China 27(2017) 1580-1587

Transactions of Nonferrous Metals Society of China

www.tnmsc.cn



Influence of Fe addition on phase transformation behavior of NiTi shape memory alloy

Yan-qiu ZHANG¹, Shu-yong JIANG¹, Xiao-ming ZHU¹, Ya-nan ZHAO¹, Yu-long LIANG², Dong SUN²

- 1. College of Mechanical and Electrical Engineering, Harbin Engineering University, Harbin 150001, China;
- 2. College of Materials Science and Chemical Engineering, Harbin Engineering University, Harbin 150001, China

Received 13 April 2016; accepted 25 October 2016

Abstract: Three different NiTi-based alloys, whose nominal compositions were Ni₅₀Ti₅₀, Ni₄₉Ti₄₉Fe₂, Ni₄₅Ti_{51.8}Fe_{3.2} (mole fraction, %), respectively, were used in the current research to understand the influence of Fe addition on phase transformation behavior in NiTi shape memory alloy (SMA). The microstructure and phase transformation behavior of the alloys were investigated by optical microscopy (OM), transmission electron microscopy (TEM), X-ray diffraction (XRD) and differential scanning calorimetry (DSC) analysis. The results show that the matrix of the Ni₅₀Ti₅₀ alloy consists of both B19' (martensite) phase and B2 (austenite) phase. Moreover, the substructures of twins could be observed in the B19' phase. However, the ternary alloys of NiTiFe exhibit B2 phase in the microstructures. Such microstructures were also characterized by large presence of Ti₂Ni precipitates dispersed homogenously in the matrix of the two kinds of alloys. The addition of Fe to the NiTi SMA results in the decrease in phase transformation temperatures in the ternary alloys. Based on mechanism analysis, it can be concluded that this phenomenon is primarily attributed to atom relaxation of the distorted lattice induced by Ni-antisite defects and Fe substitutions during phase transformation, which enables stabilization of B2 phase during phase transformation.

Key words: shape memory alloy; NiTi alloy; NiTiFe alloy; microstructure; austenite; martensite

1 Introduction

Near-equiatomic NiTi shape memory alloys (SMAs) have attracted much attention due to their unique shape excellent effect, superelasticity, mechanical properties and perfect corrosion resistance. As a result, they have become promising candidates for engineering biomedical. control and aerospace applications in recent years [1-5]. It is well known that adding a third element to replace Ni and/or Ti has a substantial effect on phase transformation behavior and microstructures of NiTi alloys. Previous studies have shown that addition of elements, such as Cu, Fe, Nb, Hf and Cr, to binary NiTi alloys satisfies some specific needs [6-10]. Among these NiTi-based alloys, NiTiFe alloys have been widely used for pipe joints owing to their excellent shape memory effect. This is attributed to the fact that the finish temperature of martensite transformation $M_{\rm f}$ of pipe joints made from NiTiFe SMA is below 0 °C and the finish temperature of austenite transformation $A_{\rm f}$ of it is lower than the room temperature. The operation principle of the pipe joint made from NiTiFe SMA is as follows. Firstly, a pipe joint whose inner diameter is smaller than the outer diameter of the two pipes is manufactured by machining. Secondly, the machined pipe joint is cooled below $M_{\rm f}$ and subsequently its inner hole is enlarged by mandrel reaming process to the size that its inner diameter is larger than the outer diameter of the pipes. Thirdly, the enlarged pipe joint is assembled with the pipes and then is heated above $A_{\rm f}$. As a consequence, the pipe joint recovers its shape and binds the pipes tightly at room temperature [11]. It has been concluded that the phase transformation temperatures of the SMAs could be lowered by Fe addition because Fe has a strong preference for entering into Ni-site and substitutes Ni [12,13]. If Fe atoms merely substitute the site of Ni atoms and exhibit the similar chemical property as Ni, their phase transformation temperatures should approximate to those of the binary NiTi SMAs. However, it has been found that phase transformation temperatures of all the NiTiFe SMAs are much lower than those of the binary NiTi SMAs according to the current references [7,13–15]. In these works, FAN et al [7] investigated the phase transformation of Ni₄₈Ti₅₀Fe₂ SMA and their that the phase transformation showed temperatures of the alloy are much smaller than those of the Ni₅₀Ti₅₀ SMA. OTSUKA and REN [13] listed the phase transformation temperatures of some NiTi-based SMAs in their article, where the phase transformation temperatures of NiTiFe SMAs are much lower than those of Ni₅₀Ti₅₀ SMA. XUE et al [14] investigated the phase transformation of Ni₄₇Ti₅₀Fe₃ SMA and their results showed that the finish temperature of austenite transformation A_f of the alloy is below 0 °C, which is lower than that of Ni₅₀Ti₅₀ SMA. CHOI et al [15] investigated the stability of the B2-type structure in a series of Ti-(50-x)Ni-xFe ($2 \le x \le 20$) alloys and found that Fe element has the ability to stabilize B2 austenite structure. However, all the literatures are related to the NiTiFe alloys with Fe substituting Ni. So far, no literatures related to the NiTiFe alloys with Fe substituting both Ti and Ni have been found.

Therefore, in the present study, the influence of Fe addition on phase transformation behavior of NiTi SMA was investigated by means of comparison among three NiTi-based alloys, whose compositions were Ni $_{50}$ Ti $_{50}$, Ni $_{49}$ Ti $_{49}$ Fe $_2$, Ni $_{45}$ Ti $_{51.8}$ Fe $_{3.2}$ (mole fraction, %), respectively, so that the mechanism of influence of Fe addition on phase transformation behavior of NiTi SMA could be revealed.

2 Experimental

Three different NiTi-based alloy ingots, whose nominal compositions were Ni₅₀Ti₅₀, Ni₄₉Ti₄₉Fe₂ and Ni₄₅Ti_{51.8}Fe_{3.2} (mole fraction, %), respectively, were prepared from 99.4 % Ti sheet, 99.98% Ni plate and 99.7% Fe slice (mass fraction) by vacuum arc melting. Each ingot was melted repeatedly for three times so as to achieve homogeneity. The as-cast ingots were placed into three quartz tubes, respectively. Afterward, they were flush with high purity argon gas for three times and then were evacuated to a pressure of about 0.1 Pa. Subsequently, the quartz tubes were sealed and then were placed into a furnace. The quartz tubes containing the ingots were heated for 12 h at 1000 °C and were quenched into ice water immediately after they were removed from the furnace. The ingots were taken out by breaking up the tubes once they were put into the ice water, so that they could be cooled as soon as possible.

In order to perform metallographic observation,

X-ray diffraction (XRD) analysis, differential scanning calorimetry (DSC) analysis and transmission electron microscopy (TEM) observation, a series of specimens were removed from the three ingots subjected to solution treatment by electro-discharge machining (EDM), respectively. The specimens for metallographic observation were etched in a solution with the $V(HF):V(HNO_3):V(H_2O)=1:2:10.$ composition of Subsequently, the metallographic morphologies were characterized by OLYMPUS311 optical microscope. Phase compositions of the alloys were obtained by XRD using an X-ray diffractometer (X-pert PRO). The phase transformations were analyzed by DSC employing a differential scanning calorimeter (Pyris Diamond DSC). The specimens for TEM observation were thinned by twin-jet polishing in an electrolyte consisting of 90% C₂H₅OH and 10% HClO₄ by volume fraction, and subsequently were observed using a FEI TECNAI G2 F30 microscope.

3 Results

3.1 Microstructure analysis

Figure 1 illustrates metallographic morphologies of the three NiTi-based alloys. It can be seen that Ni₅₀Ti₅₀ alloy is characterized by equiaxed grains and the sizes of grains are uniform. Compared with microstructures of Ni₅₀Ti₅₀ alloy in Fig. 1(a), the grain sizes of Ni₄₉Ti₄₉Fe₂ alloy are much larger and the grain boundaries of it are more curved. In addition, plenty of fine precipitates are dispersed homogeneously in the matrix of the Ni₄₉Ti₄₉Fe₂ alloy. As for the Ni₄₅Ti_{51.8}Fe_{3.2} alloy, the sizes of the grains are smaller than those of the aforementioned two alloys and the precipitates with much larger size are dispersed in the matrix.

Figures 2–4 illustrate the typical TEM photographs and the corresponding selected area diffraction (SAD) patterns of the Ni₅₀Ti₅₀ alloy, the Ni₄₉Ti₄₉Fe₂ alloy and the Ni₄₅Ti_{51.8}Fe_{3.2} alloy, respectively. In these figures, the crystal directions labeled in the lower right corner of the insets represent the crystal zone axis, which means that all the crystal planes displayed in the diffraction pattern are parallel to the crystal zone axis. The subscripts [M] and [T] stand for the crystal planes of matrix and twin, respectively, and the subscript [M,T] represents the twinning plane, where all the crystal planes are parallel to the crystal zone axes labeled in the lower right corner of the insets. It can be seen from Fig. 2 that the matrix of the Ni₅₀Ti₅₀ alloy consists of both B19' (martensite) phase and B2 (austenite) phase. Furthermore, the substructures of twins could be observed in the B19' phase, as illustrated in Figs. 2 (c) and (d). The TEM morphologies of the Ni₄₉Ti₄₉Fe₂ alloy illustrated in Fig. 3 are quite different from those of the Ni₅₀Ti₅₀ alloy. Based



Fig. 1 Metallographic morphologies of three NiTi-based SMAs: (a) Ni₅₀Ti₅₀; (b) Ni₄₉Ti₄₉Fe₂; (c) Ni₄₅Ti_{51.8}Fe_{3.2}

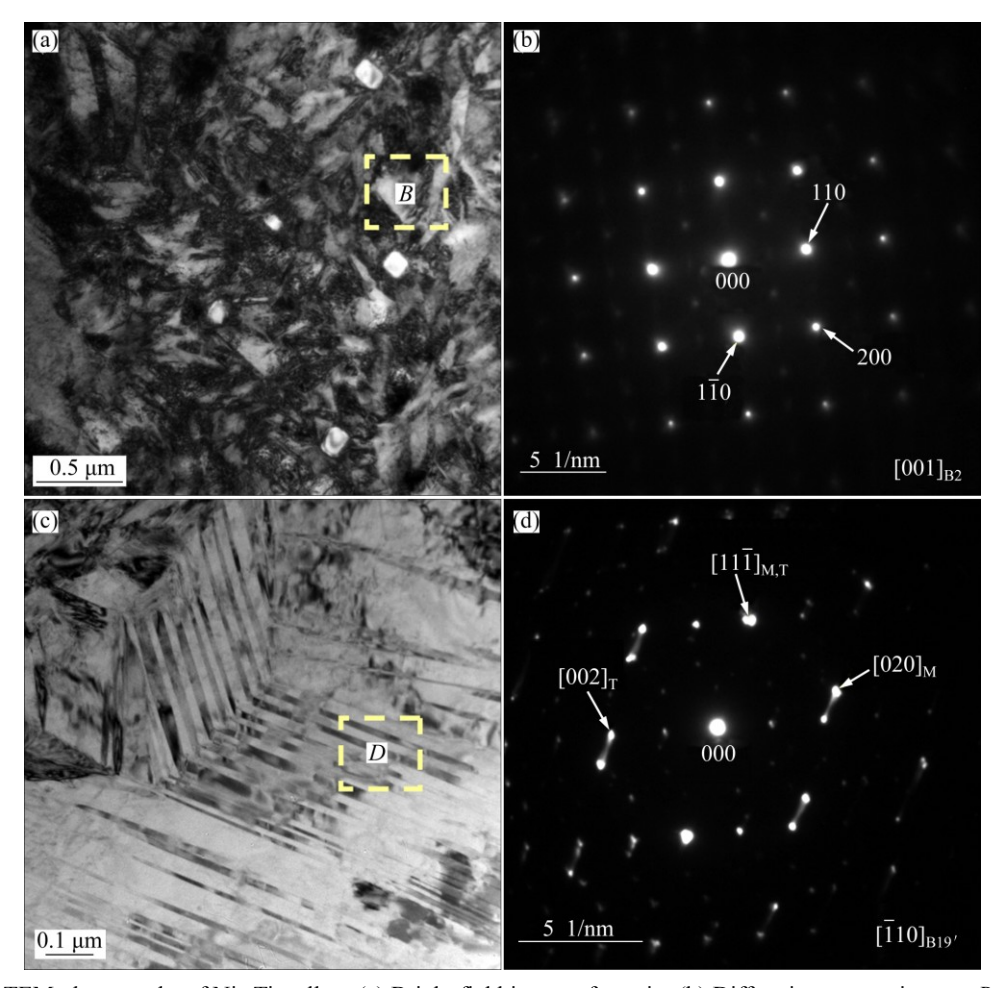


Fig. 2 Typical TEM photographs of $Ni_{50}Ti_{50}$ alloy: (a) Bright field image of matrix; (b) Diffraction pattern in zone *B* of (a), showing [001] pattern from B2 phase in matrix; (c) Bright field image showing substructures of B19' martensite in matrix; (d) Diffraction pattern in zone *D* of (c), showing $[\overline{1}10]$ pattern from B19' martensite twin

on the diffraction pattern analysis, it can be confirmed that the alloy exhibits B2 phase in the microstructures. Such microstructures are also characterized by the presence of Ti₂Ni precipitates. These Ti₂Ni precipitates appear both at the grain boundaries and in the grain interior. The Ti₂Ni precipitates arising at the grain boundaries present granular shape, while the ones appearing in the grain interior exhibit bar-like shape. It can be seen from Fig. 3(d) that there exist some dislocations in the grain interior. These dislocations may be induced by the Ti₂Ni precipitates which arouse the

stress in the matrix. It can be confirmed from Fig. 4 that the $Ni_{45}Ti_{51.8}Fe_{3.2}$ alloy exhibits B2 phase in the microstructures as well, and the microstructures are also characterized by presence of numerous Ti_2Ni precipitates dispersed homogenously. The Ti_2Ni precipitates in this alloy appear both at the grain boundaries and in the grain interior as well, but the sizes of these precipitates are much larger than those of the $Ni_{49}Ti_{49}Fe_2$ alloy. Furthermore, the morphology of the precipitate in the grain interior exhibits a peanut-like shape rather than a bar-like one.

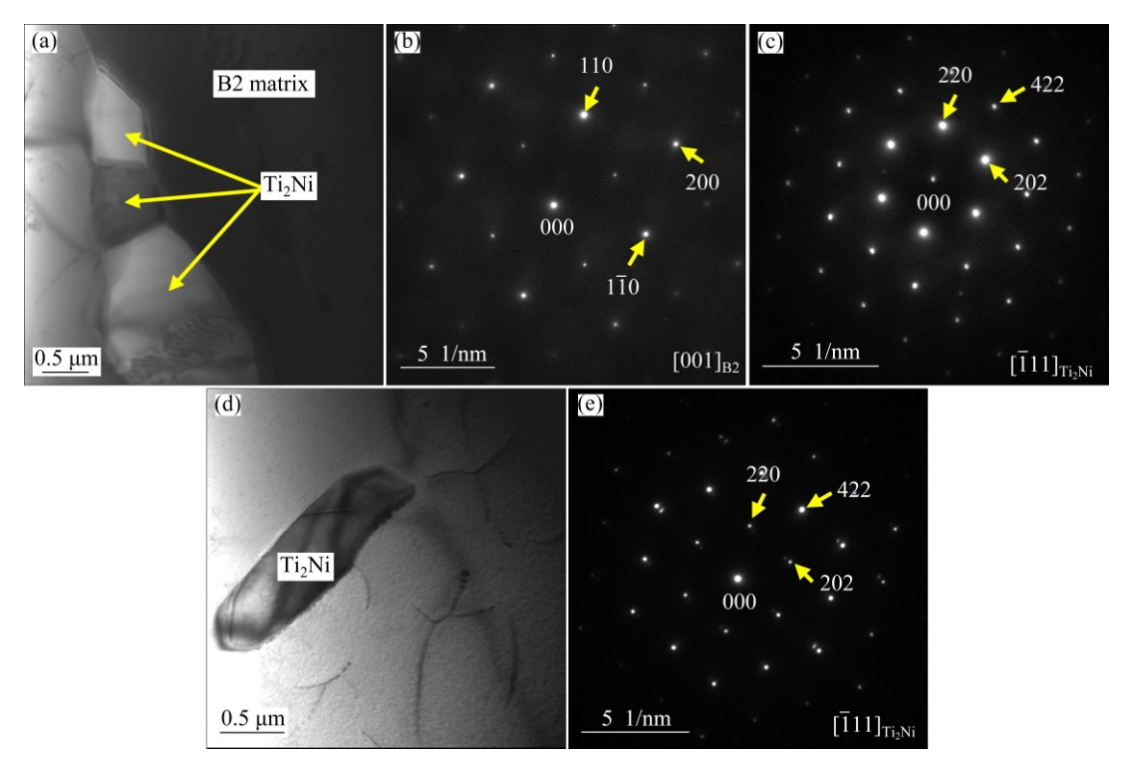


Fig. 3 Typical TEM photographs of $Ni_{49}Ti_{49}Fe_2$ alloy: (a) Bright field image showing Ti_2Ni precipitates at grain boundary of B2 matrix; (b) Diffraction pattern showing [001] pattern from B2 matrix in (a); (c) Diffraction pattern showing [$\overline{1}11$] pattern from Ti_2Ni phase in (a); (d) Bright field image showing a bar-like Ti_2Ni precipitate in grain interior of B2 matrix; (e) Diffraction pattern showing [$\overline{1}11$] pattern from Ti_2Ni precipitate in (d)

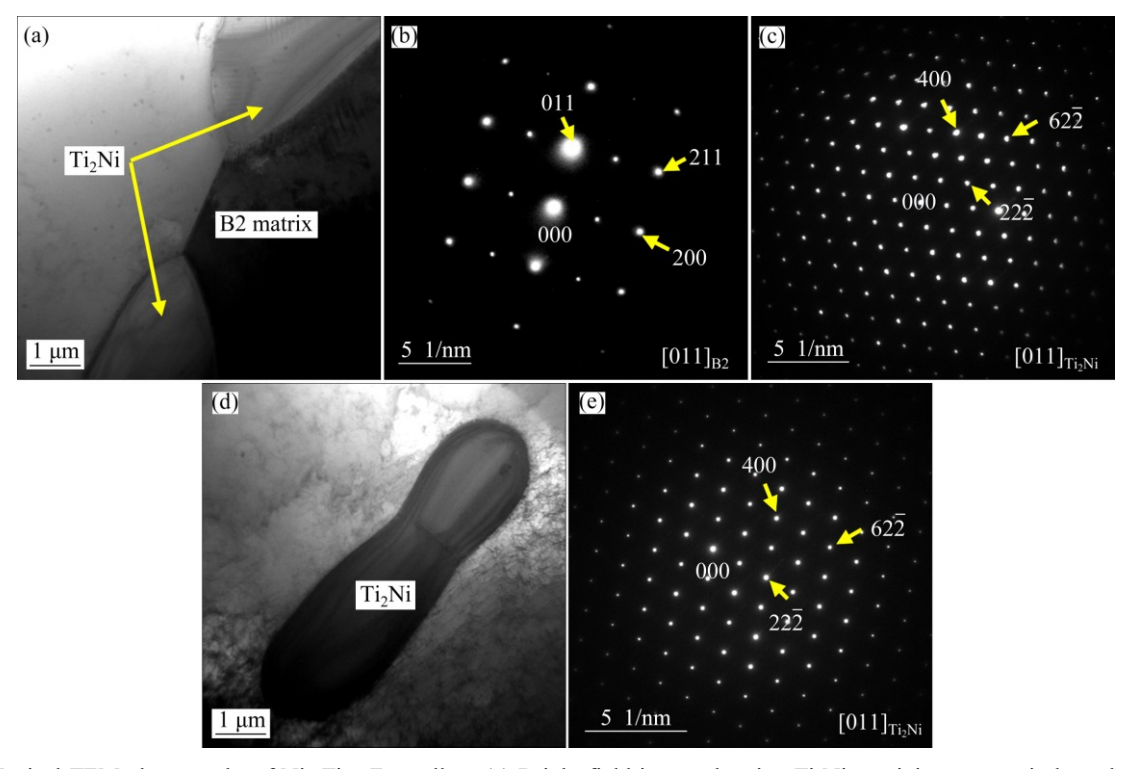


Fig. 4 Typical TEM photographs of $Ni_{45}Ti_{51.8}Fe_{3.2}$ alloy: (a) Bright field image showing Ti_2Ni precipitates at grain boundary of B2 matrix; (b) Diffraction pattern showing $[01\overline{1}]$ pattern from B2 matrix in (a); (c) Diffraction pattern showing [011] pattern from Ti_2Ni phase in (a); (d) Bright field image showing peanut-like Ti_2Ni precipitate in grain interior of B2 matrix; (e) Diffraction pattern showing [011] pattern from Ti_2Ni precipitate in (d)

3.2 XRD analysis

Phases and structures of the solution-treated NiTi-based alloys were further investigated by XRD, as shown in Fig. 5. It can be noted from Fig. 5 that the Ni₅₀Ti₅₀ alloy consists of both B2 phase and B19' phase. However, the two ternary alloys of NiTiFe consist of B2 phase and Ti₂Ni phase. Few Ti₂Ni diffraction peaks are observed in the Ni₅₀Ti₅₀ alloy because it is an equiatomic NiTi alloy. As for the Ni₄₉Ti₄₉Fe₂ alloy, very few Ti₂Ni diffraction peaks are able to be found in the XRD patterns even if plenty of Ti₂Ni precipitates are highly dispersed in the matrix, which may be attributed to the fact that Ti₂Ni precipitates are randomly oriented and each precipitate has only one reflection which is not clearly resolved. However, many Ti₂Ni diffraction peaks

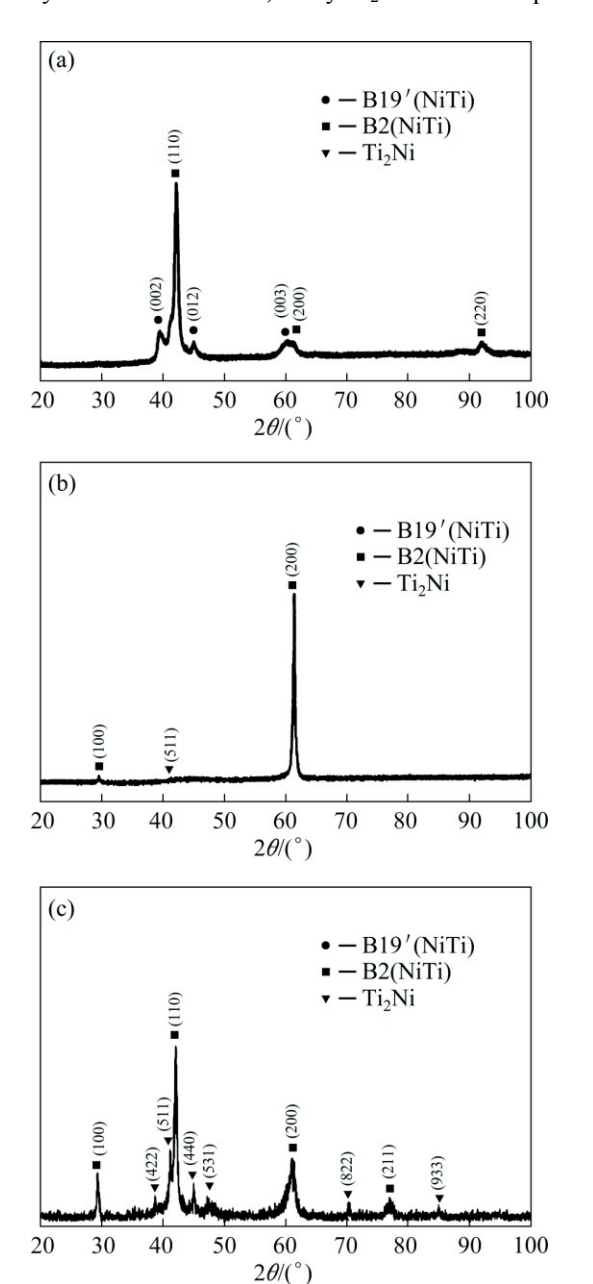


Fig. 5 XRD patterns of three NiTi-based SMAs: (a) $Ni_{50}Ti_{50}$; (b) $Ni_{49}Ti_{49}Fe_2$; (c) $Ni_{45}Ti_{51.8}Fe_{3.2}$

can be observed in the XRD patterns of $Ni_{45}Ti_{51.8}Fe_{3.2}$ alloy, which indicates that a group of Ti_2Ni precipitates have the same reflection and there exist several groups with different reflections.

3.3 DSC analysis

Figure 6 illustrates the DSC curves of the three NiTi-based SMAs. It can be seen from Fig. 6(a) that there exist two peaks in the DSC curve of Ni₅₀Ti₅₀ alloy, where the exothermic peak during cooling corresponds to the transformation from austenitic phase to martensitic phase (A \rightarrow M) and the endothermic peak during heating corresponds to the transformation from martensitic phase to austenitic phase (M \rightarrow A). Based on the DSC curve, phase transformation temperatures of the Ni₅₀Ti₅₀ alloy were determined as M_s =37.4 °C, M_f =13.4 °C, A_s =46.2 °C and A_f =68.3 °C, which is consistent with the XRD results in Fig. 5(a), where B2 phase and B19' phase coexist at room temperature. It is curious that no peak arises in the DSC curve of the Ni₄₉Ti₄₉Fe₂ alloy, as shown in Fig. 6(b). This phenomenon demonstrates that phase

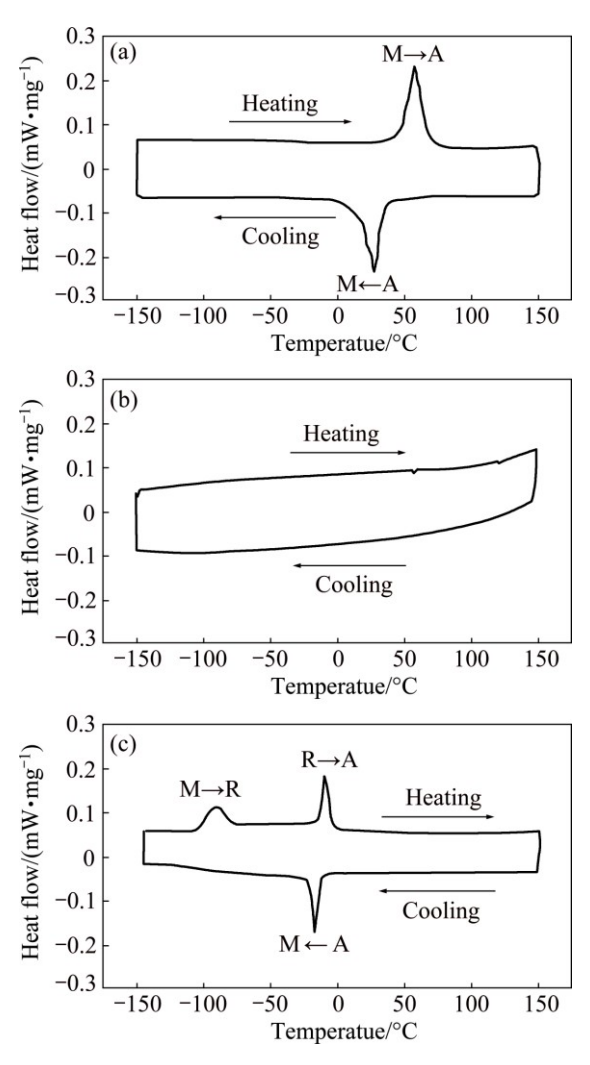


Fig. 6 DSC curves of three NiTi-based SMAs: (a) $Ni_{50}Ti_{50}$; (b) $Ni_{49}Ti_{49}Fe_2$; (c) $Ni_{45}Ti_{51.8}Fe_{3.2}$

transformation temperatures of the alloy are out of the range of current testing temperature. In other words, the phase transformation temperatures are lower than −150 °C. It has been proved that Fe has a strong preference for entering into Ni-site and substitutes Ni because it has similar chemical property as Ni [12,13]. Therefore, the phase transformation temperatures of Ni₄₉Ti₄₉Fe₂ alloy should be theoretically close to those of Ni₅₁Ti₄₉ alloy. However, the martensitic transformation temperature M_s of the $Ni_{49}Ti_{49}Fe_2$ alloy in the present study is much lower than that of $Ni_{51}Ti_{49}$ alloy, whose M_s is about -120 °C according to Ref. [13]. Furthermore, it can be seen from Fig. 6(c) that the phase transformation temperatures of the Ni₄₅Ti_{51.8}Fe_{3.2} alloy are much lower than those of the equiatomic Ni₅₀Ti₅₀ alloy. In theory, the phase transformation temperatures of the Ni₄₅Ti_{51.8}Fe_{3.2} alloy should be close to those of the Ni_{48.2}Ti_{51.8} alloy, whose martensitic transformation temperature M_s should be no less than that of the equiatomic Ni₅₀Ti₅₀ alloy due to its Ti-rich composition [13]. Therefore, it can be concluded from Figs. 6(b) and (c) that the influence of Fe addition on the phase transformation temperatures is much larger than that of Ni addition. However, the reason why the phenomenon takes place has not been found in the current literatures.

It can be also seen from Fig. 6(c) that there exist three peaks in the DSC curve, where the exothermic peak during cooling corresponds to the transformation from austenitic phase to martensitic phase (A

M) and the two endothermic peaks during heating correspond to the transformation from martensitic phase to R phase (M→R) and the one from R phase to austenitic phase $(R \rightarrow A)$, respectively. This phenomenon is different from the results described in previous investigations, where R phase transformation occurs during cooling alone or during both cooling and heating [16,17]. The occurrence of the multi-stage transformation in this case may be attributed to the formation of coherent Ti₂Ni precipitates, which creates local stress fields [18,19]. However, the mechanism inducing the multi-stage transformation has not been evident yet and will be investigated in the future.

4 Discussion

It has been reported that the major defect in the off-stoichiometric NiTi SMA is antisite defect, which results from the atoms that are located in wrong sites [20]. For the Ni-rich binary NiTi alloy, excess Ni atoms occupy Ti lattice sites of B2 matrix and the slightly off-stoichiometric B2 phase is stabilized through the formation of antisite defects. Once the antisite defects are formed, the lattices where the defect is located will be distorted because there exists atom size difference

between the two elements. Consequently, the atoms in the distorted lattice tend to return to their force-free positions during phase transformation. This phenomenon is determined as atomic relaxation, which has a strong effect on the energy difference between B2 phase and B19' phase. These large local displacements of the atoms in the neighborhood of the Ni-antisite atom are associated with a significant energy gain during the atomic relaxation and thus lead to the stabilization of the Ni-rich B2 phase [21]. Therefore, the martensitic transformation temperature M_s of the Ni-rich binary NiTi SMA is lowered due to the stabilization of B2 phase. It has been confirmed by BOZZOLO et al [12] that Fe atoms prefer to occupy the Ni site rather than occupy the Ti site in the NiTiFe alloy. Therefore, in the case of ternary NiTiFe alloy, the lattices of B2 phase are further distorted by the larger Fe atoms when the body-centered positions which Ni atoms are located in are replaced by the Fe atoms. The Ti atoms around the Fe atoms also tend to return to their force-free positions, and hence atomic relaxation occurs in these Ti atoms during the phase transformation as well. As a consequence, the B2 phase is further stabilized by the atomic relaxation around the Fe atoms and hence M_s is further lowered as compared to corresponding binary NiTi SMA. Figures 7(a)–(c) illustrate the undistorted lattices, the relaxation of distorted lattices with a Ni-antisite defect and the relaxation of distorted lattices with a Fe atom substitution, respectively. Figure 7(d) shows the diagram of martensite transformation for the Ni₅₀Ti₅₀ alloy, where B2 matrix directly transforms into B19' matrix through shearing because there is no distortion of lattices. Figure 7(e) shows the diagram of martensite transformation for the Ni₄₅Ti_{51.8}Fe_{3.2} alloy, where both atom relaxation around Ni-antisite defects and the atom relaxation around Fe atoms occur prior to the martensite transformation. These relaxations stabilize the B2 phase and hence decrease the martensitic transformation temperature. As Ti-rich binary NiTi alloy, the phase transformation temperatures are much less sensitive to the composition due to the precipitation of Ti₂Ni particles, which leaves the composition of the B2 matrix relatively unchanged and hence the phase transformation temperatures of the Ti-rich NiTi alloy are close to those of equiatomic NiTi alloy [13]. However, lattices in the B2 matrix are distorted in the Ti-rich NiTiFe alloy because Fe atoms substitute some Ni atoms. The B2 phase is stabilized by the atom relaxation around the Fe atoms and hence the phase transformation temperatures are lowered as compared to corresponding binary NiTi SMA. Therefore, only one lattice relaxation mode, i.e., the atom relaxation around Fe atoms, is dominant in the Ti-rich NiTiFe SMA, as shown in Fig. 7(f).

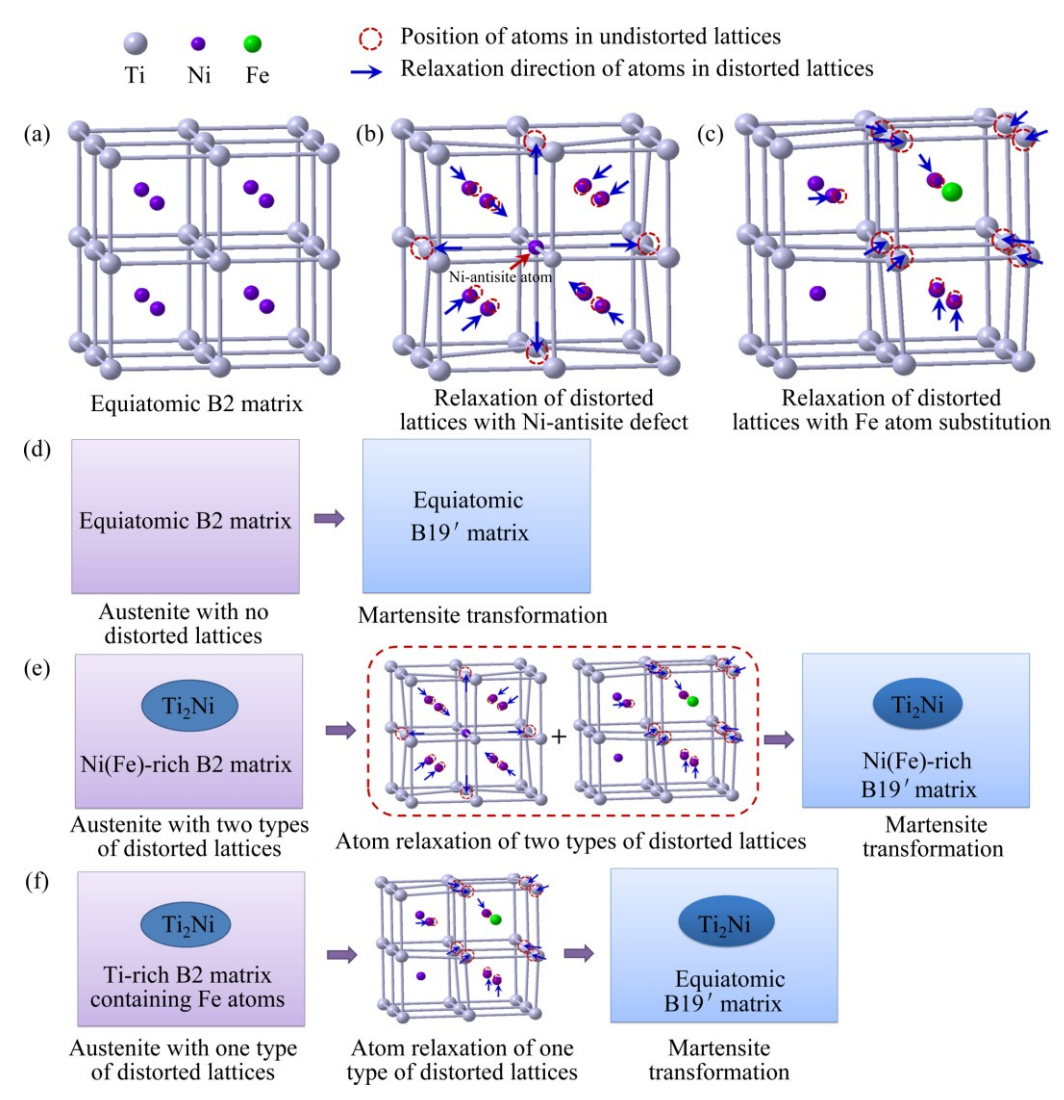


Fig. 7 Mechanism diagram of influence of Fe addition on phase transformation of NiTi SMAs: (a) Undistorted B2 lattices; (b) Relaxation of distorted lattices with Ni-antisite defect; (c) Relaxation of distorted lattices with Fe atom substitution; (d) Phase transformation process of equiatomic Ni₅₀Ti₅₀ alloy; (e) Phase transformation process of Ni₄₉Ti₄₉Fe₂ alloy; (f) Phase transformation process of Ni₄₅Ti_{51.8}Fe_{3.2} alloy

5 Conclusions

- 1) The matrix of the $Ni_{50}Ti_{50}$ alloy consists of B19′ (martensite) phase and B2 (austenite phase), and the substructures of twins could be observed in the B19′ phase. However, the ternary alloys of NiTiFe exhibited B2 phase in the microstructures. Such microstructures were also characterized by presence of numerous Ti_2Ni precipitates dispersed homogenously in the matrix of the two kinds of alloys.
- 2) Adding Fe element to the NiTi SMA results in the decrease of phase transformation temperatures of the ternary alloys of NiTiFe as compared to the binary NiTi SMA involved. This phenomenon is primarily attributed to atom relaxation of the distorted lattice induced by Ni-antisite defects and Fe substitutions during phase

transformation. The atom relaxation is associated with a significant energy gain and thus leads to the stabilization of the B2 phase. The lattice relaxation in the Ni(Fe)-rich NiTiFe alloys is regarded as the superposition of two modes, which include atom relaxation around Ni-antisite defects and the atom relaxation around Fe atoms. However, only one lattice relaxation mode, namely the atom relaxation around Fe atoms, is considered to be dominant in the Ti-rich NiTiFe alloy.

References

- JIANG Shu-yong, HU Li, ZHAO Ya-nan, ZHANG Yan-qiu, LIANG Yu-long. Plastic yielding of NiTi shape memory alloy under local canning compression [J]. Transactions of Nonferrous Metals Society of China. 2013. 23: 2905–2913.
- [2] JIANG Shu-yong, TANG Ming, ZHAO Ya-nan, HU Li, ZHANG Yan-qiu, LIANG Yu-long. Crystallization of amorphous NiTi shape

- memory alloy fabricated by severe plastic deformation [J]. Transactions of Nonferrous Metals Society of China, 2014, 24: 1758–1765
- [3] JIANG Shu-yong, ZHANG Yan-qiu, ZHAO Ya-nan, LIU Si-wei, HU Li, ZHAO Cheng-zhi. Influence of Ni₄Ti₃ precipitates on phase transformation of NiTi shape memory alloy [J]. Transactions of Nonferrous Metals Society of China, 2015, 25: 4063–4071.
- [4] ZHANG Yan-qiu, JIANG Shu-yong, ZHAO Ya-nan, LIU Si-wei. Constitutive equation and processing map of equiatomic NiTi shape memory alloy under hot plastic deformation [J]. Transactions of Nonferrous Metals Society of China, 2016, 26: 2152–2161.
- [5] JIANG Shu-yong, TANG Ming, ZHAO Ya-nan, HU Li, ZHANG Yan-qiu, LIANG Yu-long. Crystallization of amorphous NiTi shape memory alloy fabricated by severe plastic deformation [J]. Transactions of Nonferrous Metals Society of China, 2014, 24: 1758–1765.
- [6] SINGH N, TALAPATRA A, JUNKAEW A, DUONG T, GIBBONS S, LI S, THAWABI H, OLIVOS E, ARRÓYAVE R. Effect of ternary additions to structural properties of NiTi alloys [J]. Computational Materials Science, 2016, 112: 347–355.
- [7] FAN G, ZHOU Y, OTSUKA K, REN X, SUZUKI T, YIN F. Comparison of the two relaxation peaks in the Ti₅₀Ni₄₈Fe₂ alloy [J]. Materials Science and Engineering: A, 2009, 521-522: 178-181.
- [8] BEWERSE C, BRINSON L C, DUNAND D C. Microstructure and mechanical properties of as-cast quasibinary NiTi-Nb eutectic alloy [J]. Materials Science and Engineering: A, 2015, 627: 360-368.
- [9] HORNBUCKLE B C, NOEBE R D, THOMPSON G B. Influence of Hf solute additions on the precipitation and hardenability in Ni-rich NiTi alloys [J]. Journal of Alloys and Compounds, 2015, 640: 449–454.
- [10] HSIEH S F, CHEN S L, LINC H C, LIN M H, HUANG J H, LIN M C. A study of TiNiCr ternary shape memory alloys [J]. Journal of Alloys and Compounds, 2010, 494: 155–160.
- [11] FUNAKUBO H. Shape memory alloys [M]. New York: Gordon and Breach Science Publishers, 1987.
- [12] BOZZOLO G, NOEBE R D, MOSCA H O. Site preference of ternary

- alloying additions to NiTi: Fe, Pt, Pd, Au, Al, Cu, Zr and Hf [J]. Journal of Alloys and Compounds, 2005, 389: 80–94.
- [13] OTSUKA K, REN X. Physical metallurgy of Ti–Ni-based shape memory alloys [J]. Progress in Materials Science, 2005, 50: 511–678.
- [14] XUE S, WANG W, WU D, ZHAI Q, ZHENG H. On the explanation for the time-dependence of B2 to R martensitic transformation in Ti₅₀Ni₄₇Fe₃ shape memory alloy [J]. Materials Letters, 2012, 72: 119–121.
- [15] CHOI M S, OGAWA J, FUKUDA T, KAKESHITA T. Stability of the B2-type structure and R-phase transformation behavior of Fe or Co doped Ti–Ni alloys [J]. Materials Science and Engineering A, 2006, 438–440: 527–530.
- [16] NAGASE T, SASAKI A, YASUDA H Y, MORI H, TERAI T, KAKESHITA T. Stability of B2 phase in TiNiFe alloys against MeV electron-irradiation-induced solid-state amorphization and martensite transformation [J]. Intermetallics, 2011, 19: 1313–1318.
- [17] MIYAZAKI S, OTSUKA K. Mechanical behaviour associated with the premartensitic rhombohedral-phase transition in a Ti₅₀Ni₄₇Fe₃ alloy [J]. Philosophical Magazine A, 1984, 50: 393–408.
- [18] NAM T H, KIM J H, CHOI M S, LEE H W, KIM Y W, IM H J, AHN J, MITANI T. Effect of alloy compositions on the R phase transformation in Ti-Ni alloy ribbons fabricated by rapid solidification [J]. Journal of Materials Science Letters, 2002, 21: 799–801
- [19] LIU Y, BLANC M, TAN G, KIM J I, MIYAZAKI S. Effect of ageing on the transformation behaviour of Ti-49.5 at.% Ni [J]. Materials Science and Engineering: A, 2006, 438-440: 617-621.
- [20] KOGACHI M, HARAGUCHI T. Possibilities of random vacancy distribution and antisite atom recovering in the point defect mechanism in B2-type intermetallics [J]. Intermetallics, 1999, 7: 981–793.
- [21] FRENZEL J, WIECZOREK A, OPAHLE I, MAAß B, DRAUTZ R, EGGELER G. On the effect of alloy composition on martensite start temperatures and latent heats in Ni-Ti-based shape memory alloys [J]. Acta Materialia, 2015, 90: 213-331.

Fe 的添加对 NiTi 形状记忆合金相变行为的影响

张艳秋1,江树勇1,朱晓明1,赵亚楠1,梁玉龙2,孙冬2

- 1. 哈尔滨工程大学 机电工程学院,哈尔滨 150001;
- 2. 哈尔滨工程大学 材料科学与化学工程学院,哈尔滨 150001

摘 要:制备了三种名义成分分别为 Ni₅₀Ti₅₀、Ni₄₉Ti₄₉Fe₂和 Ni₄₅Ti_{51.8}Fe_{3.2} (摩尔分数,%)的不同 NiTi 基合金来揭示 Fe 的添加对 NiTi 形状记忆合金相变行为的影响。采用光学显微分析法、透射电子显微分析法、X 射线衍射和 差示扫描量热法对这些合金的组织和相变行为进行分析。结果表明,Ni₅₀Ti₅₀ 合金的基体由 B19′马氏体相和 B2 奥氏体相组成。而且,在 B19′相中可以观察到孪晶亚结构。然而,三元 NiTiFe 合金的组织则为 B2 奥氏体相。这两种合金的基体中弥散分布着大量的 Ti₂Ni 沉淀相。NiTi 形状记忆合金中添加 Fe 后导致三元合金的相变温度下降。由机理分析可以得到如下结论:这一现象主要是由原子的弛豫引起的,弛豫会导致相变过程中 B2 相的稳定化。 关键词:形状记忆合金;NiTi 合金;NiTiFe 合金;显微结构;奥氏体;马氏体

(Edited by Yun-bin HE)